Inorganic Chemistry

Article

pubs.acs.org/IC

Raman Spectroscopic and ESI-MS Characterization of Uranyl Peroxide Cage Clusters

Brendan T. McGrail,[†] Ginger E. Sigmon,[†] Laurent J. Jouffret,[†] Christopher R. Andrews,[†] and Peter C. Burns*[,†,‡]

[†]Department of Civil and Environmental Engineering and Earth Sciences, University of Notre Dame, Notre Dame, Indiana 46556, United States

[‡]Department of Chemistry and Biochemistry, University of Notre Dame, Notre Dame, Indiana 46556, United States

Supporting Information

ABSTRACT: Strategies for interpreting mass spectrometric and Raman spectroscopic data have been developed to study the structure and reactivity of uranyl peroxide cage clusters in aqueous solution. We demonstrate the efficacy of these methods using the three best-characterized uranyl peroxide clusters, $\{U_{24}\}$, $\{U_{28}\}$, and $\{U_{60}\}$. Specifically, we show a correlation between uranyl−peroxo−uranyl dihedral bond angles and the position of the Raman band of the symmetric stretching mode of the peroxo ligand, develop methods for the assignment of the ESI mass spectra of uranyl peroxide cage clusters, and show that these methods are generally applicable for detecting these clusters in the solid state and solution and for extracting information about their bonding and composition without crystallization.

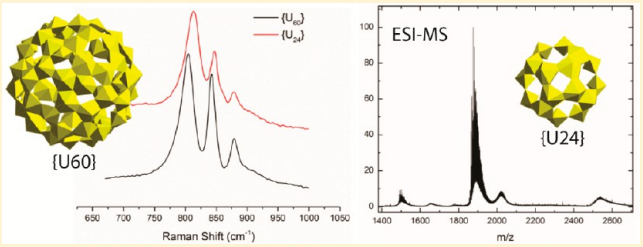

INTRODUCTION

The development of physical organic chemistry in the midtwentieth century has put much of the chemical and materials industries on sound scientific footing by enabling the rational synthesis of drugs, materials, and commodity chemicals and by developing quantitative relationships between the structures of organic molecules and their reactivity and other physical properties. The speed with which physical organic chemistry developed from unexplored terrain to a major commercial enterprise is largely attributable to the development of quantitative spectroscopic methods, first, UV−visible and infrared (IR) in the 1920s and 1930s and, later, nuclear magnetic resonance (NMR) in the 1960s and 1970s.[1] These techniques, and especially the high receptivity and useful abundances of the spin 1/2 nuclei ^{1}H and ^{13}C, enabled thorough kinetic study and even direct observations of unisolable intermediates, while the well-established methods of organic synthesis enabled the preparation of model compounds for study.[1,2]

Relative to the above-mentioned examples, polyoxometalate (POM) chemistry has not benefited as much from non-solid-state characterization approaches. While several effective preparative routes to the classical Keggin, Lindqvist, and Wells−Dawson ions exist,[3] and NMR has been effective for studying the isomerization and fundamental reactivity of POMs[4−9] using the ^{183}W, ^{51}V, and ^{17}O nuclei, the utility of ^{95}Mo, ^{97}Mo, ^{93}Nb, and ^{181}Ta NMR spectroscopy is limited by poor receptivity, large nuclear quadrupole moments, paramagnetism of the clusters, or a combination of these, and the high cost of ^{17}O enrichment renders it unsuitable for routine analysis.[10,11]

The traditional method of verifying POM structures is the growth of single crystals suitable for structure determination by X-ray diffraction, which, in addition to being unsuitable for analysis of reaction mixtures, is slow, laborious, and limits work to crystallizable POMs. Mass spectrometry, especially with electrospray ionization sources (ESI-MS), has found extensive use in POM chemistry in the study of reaction mixtures,[11−14] gas-phase dissociation pathways, and structure-fragment relationships[15−18] and as a method for "fingerprinting" POMs and POM-based supramolecules.[11,19]

We are particularly interested in understanding the mechanisms of self-assembly of the broad family of uranyl peroxide nanoscale cage clusters that form in aqueous solution (e.g., Figure 1, Table 1).[40] While ESI-MS of transition-metal POMs has been steadily developing over the past decade,[11−14] and the mass spectrum of $\{U_{60}\}$ has been reported,[19] an appreciation of how uranyl peroxide cage clusters behave under ESI-MS conditions is lacking, holding back study of the reactivity of these molecules. To complement mass spectrometric methods, we have also examined trends in the Raman spectra of several reported uranyl peroxide clusters, including some that are only available in low yields, to provide a method for extracting rudimentary structural information from Raman spectra of solutions or solids where single crystals cannot be grown but the nuclearity and purity of a cluster can be verified

Received: October 10, 2013
Published: January 14, 2014

   dx.doi.org/10.1021/ic402570b | Inorg. Chem. 2014, 53, 1562−1569

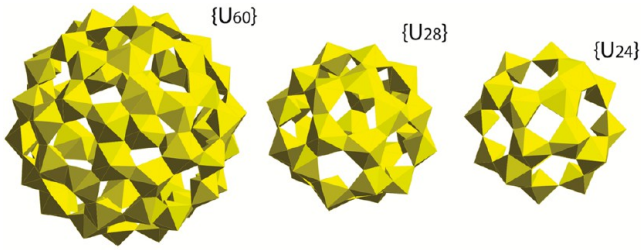

Figure 1. Polyhedral representations of $\{U_{60}\}$, $\{U_{28}\}$, and $\{U_{24}\}$. U - yellow.

by ESI-MS. We have limited this study to unsubstituted uranyl peroxide clusters (that is, isopoly(per)oxometalates containing only uranium and oxygen in the cage structure). Although many substituted clusters (heteropoly(per)oxometalates) exist,[20] we have not extended these methods to those systems at this point.

EXPERIMENTAL SECTION

Caution! *Although depleted uranium was used in these experiments, it is radioactive and should only be handled by qualified personnel in appropriate facilities.*

General Considerations. Uranyl nitrate hexahydrate ($UO_2(NO_3)_2{\cdot}6H_2O$) was purchased from International Bio-Analytical Industries, Inc. and purified by conversion to UO_3 at 450 °C, followed by dissolution in concentrated HNO_3. The resulting solution was evaporated to dryness by boiling on a hot plate, and the yellow powder so-obtained was purified by recrystallization from ultrapure water. All other reagents were purchased from commercial suppliers and used as received. Additional reagents added to cluster solutions were added as solids to known volumes of solution to produce the concentrations noted. Clusters are denoted as $\{U_n\}$, where n is the number of $[UO_2(O_2)(OH)]^-$ or $[UO_2(O_2)_{1.5}]^-$ units in the cluster.[20] Cluster fragments observed by mass spectrometry, but not isolable as crystalline solids, are denoted using this system as well. Raman data from extended structures are included in Figure 3, but are excluded from the cluster-only data given in Figure 2.

Synthesis of $Li_{24}\{U_{24}\}{\cdot}xH_2O$. Hydrogen peroxide (1.9 mL, 30% aqueous) was added to 15 mL of 0.25 M aqueous $UO_2(NO_3)_2$ with vigorous stirring to give a pale yellow precipitate. Stirring was maintained while 8.75 mL of 3.0 M LiOH was added in ca. 1 mL increments while stirring continued. The precipitate dissolved with evolution of a gas, and afforded an orange solution. This solution was stirred covered for 60 min, giving a final solution pH between 9 and 9.2. If this pH was not attained after ca. 60 min, 2 M HCl was added dropwise until the pH was attained. The solution was then uncovered and allowed to evaporate to dryness in a fume hood with continuous stirring. The material so-obtained was redissolved in 10 mL of deionized water, filtered through a medium frit, and covered with a watch glass for 10 days, at which point it was uncovered and allowed to evaporate to dryness on the benchtop. The resultant yellow powder was washed with 70/30 (v/v) water/acetonitrile (2 × 5 mL) and water (2 × 3 mL) to remove side products (principally $LiNO_3$ and excess LiOH). The washed material was redissolved in 5 mL of water, stirred covered overnight, and filtered through a 0.2 μm PTFE syringe filter to remove aggregated material. Aggregated material could also be removed by centrifugation at 7500 rpm for 2 min and decanting the supernatant, albeit with lower yields. This solution was then evaporated overnight by vigorous stirring uncovered at 35 °C in a fume hood, giving material of adequate purity for further study. Recrystallization from a minimal amount of water (ca. 4 mL) by slow evaporation afforded a larger collection of diffraction-quality single crystals. The diffraction-quality single crystals are spectroscopically and spectrometically identical to the washed powder, and crystal structure determination by single-crystal X-ray diffraction confirms the identity of the product as $\{U_{24}\}$, in agreement with previous literature reports.[24] Yield: 0.873 g (76% based on U). Raman (H_2O): 813 cm^{-1} (s, O-U-O), 843 cm^{-1} (m, O-O), 878 cm^{-1} (m, O-O). R_g (SAXS, Guinier): 0.79 nm. UV−vis (H_2O): λ/nm $\{\varepsilon(M^{-1}\ cm^{-1})\}$ 197 {63455}, 232 (sh) {40105}. Anal. Calcd for $Li_{24}[UO_2(O_2)(OH)]_{24}$ (7825.18) U: 0.729 Li: 0.0213; found U: 0.727, Li: 0.024.

Synthesis of Other Clusters. Other uranyl peroxide clusters were prepared in, and crystallized from, aqueous solution according to literature procedures. $\{U_{28}\}$ (as the K^+/Rb^+ salt) was prepared by the method of Nyman.[21] Sufficient quantities of $\{U_{60}\}$ are not available in large one-pot synthesis, and instead, several small reactions were run according to the method given by Armstrong et al.[19] Published methods for the preparation of other clusters[22−26] afforded only a few single crystals that were isolated under an optical microscope and verified by determination of unit cells using single-crystal X-ray diffraction. In this study, we collected the solid-state Raman spectra of the clusters $\{U_{20}\}$, $\{U_{36}\}$, $\{U_{32R}\}$, $\{U_{44}\}$, and $\{U_{24R}\}$, a previously reported uranyl peroxide sheet material[27] and a synthetic analogue of the mineral studtite.[28]

Raman Spectroscopy. Raman spectra were acquired using a Bruker Sentinel system equipped with a fiber optic probe, thermoelectric cooled CCD detector, and a 785 nm excitation source. Spectra of solid samples were acquired from 80 to 3200 cm^{-1} using five 2 s exposures at 100−250 mW laser power on single crystals isolated under a Nikon optical microscope attached to the Raman probe. The minimum power required to get adequate signal-to-noise in the spectra was used to minimize sample damage. We also collected spectra for purified uranyl peroxide clusters in aqueous solution. These spectra were acquired from 80 to 3200 cm^{-1} by averaging three 15 s exposures at 400 mW laser power. Solutions were prepared by dissolving purified cluster crystals or powders in ultrapure water.

Electrospray Ionization-Mass Spectrometry. ESI mass spectra were acquired using a Bruker qTOF time-of-flight spectrometer or a Waters (MicroMass) triple quadrupole spectrometer. Samples were prepared to 5−20 μM concentration and directly infused into the ionization sources using syringe pumps at flow rates between 5 and 25 μL/min. TOF data were acquired at a capillary voltage of 3600 V, an end plate offset of −500 V, 0.8 bar dry gas, 1.2 L/min desolvation gas, and 200 °C dry gas temperature. Triple quadrupole mass spectra were acquired at a capillary voltage of 2.20 kV, a cone voltage of 18 V, RF cone at 0.3, 80−90 L/h nebulizer gas, 400−420 L/h desolvation gas, a source temperature of 120 °C, and a desolvation temperature of 225 °C. Tandem MS (MS/MS) data were acquired with entrance and exit voltages of 50 V and Ar as the collision gas. Collision voltages for MS/MS were varied from 0 to 50 V in 5 V increments. Dinitrogen was used as the desolvation and nebulizer gases for both instruments. Mass spectra are simulated using Molecular Weight Calculator 6.49 for Windows.[29]

RESULTS AND DISCUSSION

Raman Spectroscopy. The single-crystal Raman spectra of all uranyl peroxide clusters examined here show two prominent bands (Figure 2): the first in the range of 800−820 cm^{-1} and the second in the range of 820−850 cm^{-1}. In an attempt to make definitive assignments of these bands, we examined the

Table 1. Formulae of Clusters Used for ESI-MS Study with H_2O of Crystallization Omitted

cluster		
$\{U_{24}\}$	$\{U_{28}\}$	$\{U_{60}\}$
$Li_{24}[UO_2(O_2)(OH)]_{24}{\cdot}a$LiCl$\cdot b$LiNO$_3$	$Rb_{16}K_{3.5}[UO_2(O_2)_{1.5}]_{28}{\cdot}a$(Rb,K)Cl$\cdot$(Rb,K)NO$_3$	$Li_{48}K_{12}[UO_2(O_2)(OH)]_{24}{\cdot}a$(Li,K)Cl$\cdot b$(Li,K)NO$_3$

dx.doi.org/10.1021/ic402570b | Inorg. Chem. 2014, 53, 1562−1569

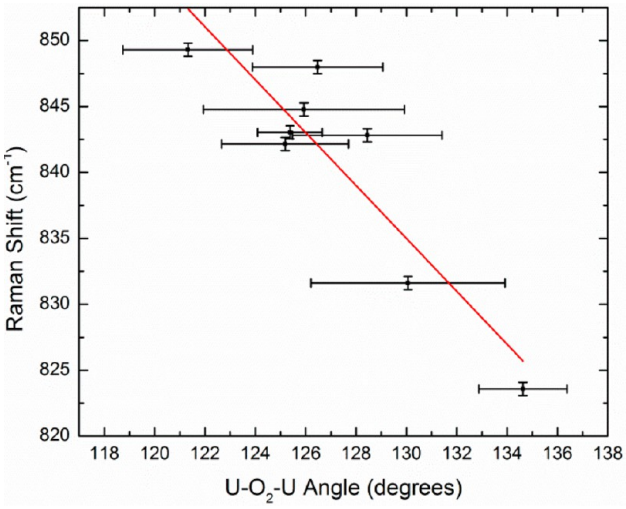

Figure 2. Plot of the 820−850 cm^{-1} band position against the mean in-plane uranium−peroxo−uranium dihedral angle in uranyl peroxide cage clusters. Horizontal error bars represent one standard deviation in the bond angles within a given cluster. Vertical error bars represent instrumental resolution.

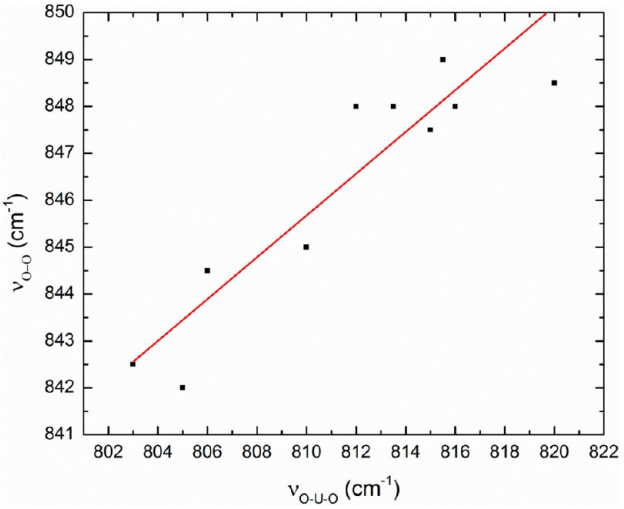

Figure 3. Relationship between the uranyl symmetric stretching mode and peroxide O−O symmetric stretching mode. The red line represents the least-squares best fit to the points. Errors are smaller than the data points.

crystallographic data available for each cluster to extract U−O bond lengths and cluster U−O_2−U dihedral angles for peroxide bridges.

The band in the range of 800−820 cm^{-1} shows little or no correlation with any geometric parameters from the corresponding structures, but is commonly assigned to the symmetric stretching mode of the uranyl ion. In contrast, the frequency of the band in the range of 820−850 cm^{-1} exhibits a good correlation (R^2 = 0.797) with the average U−O_2−U dihedral angle of the corresponding cluster (Figure 2). This correlation is the basis for assigning the 820−850 cm^{-1} band to the O−O symmetric stretching mode (ν_{O-O}) of the μ:η^2-η^2 peroxo ligand, in line with the assignment made for the same mode in studtite by Griffith et al. on the basis of isotopic labeling studies.[30] The lower energy band is assigned to the symmetric stretching mode of the uranyl ion ($\nu_{s,\ O-U-O}$) based on its correlation with the Raman shift of the O−O symmetric stretching mode (R^2 = 0.833, Figure 3) and after Komyak et al. and Griffith et al.[30,31] The observed correlation of the band position with the O−O stretching mode strengthens this assignment, and coupled with the observed poor correlation with the U−O_{yl} bond lengths, suggests significant covalency in the uranyl−peroxide interaction, consistent with density functional theory (DFT) simulations.[32−35]

As expected, the Raman spectra of uranyl peroxide clusters in aqueous solution (Figure 4) are similar to the solid-state Raman spectra, although the 878 cm^{-1} band is severely attenuated in both spectra. This attenuation will be addressed below. {U_{60}} and {U_{24}} each show three bands in their solution-phase Raman spectra. The positions of the two lowest-frequency bands are essentially unchanged relative to those of the solid state to within the instrumental resolution of ±1 cm^{-1}, although they are broadened by 5−10 cm^{-1}, suggesting some degree of conformational nonrigidity for the clusters in solution. This nonrigidity has been observed by NMR for the pyrophosphate substituted cluster $[UO_2(O_2)(P_2O_7H)_{0.5}]_{24}^{36-}$ ({$U_{24}Pp_{12}$}).[36] The third band, which is at 878 cm^{-1} for each cluster, is noteworthy for being at a higher frequency than even uncoordinated hydrogen peroxide or the hydroperoxide

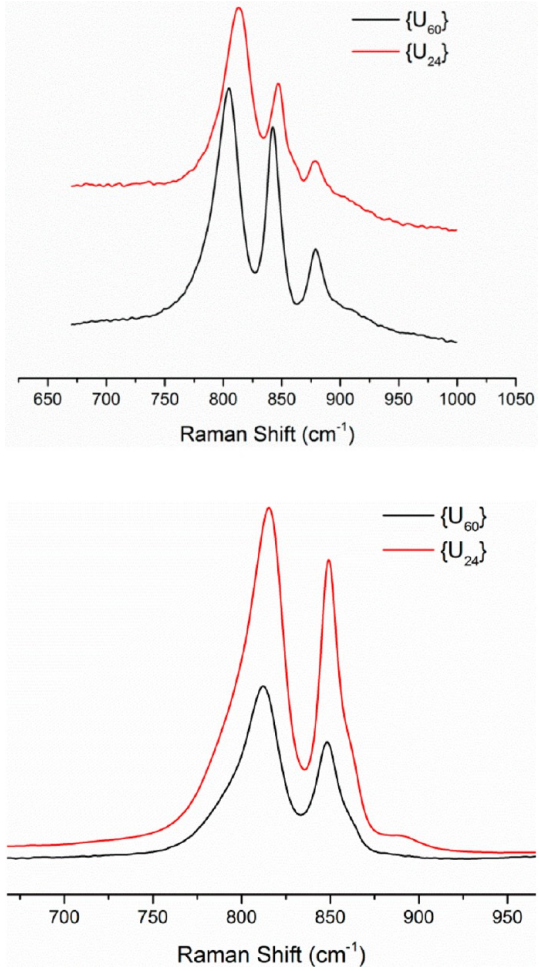

Figure 4. Raman spectra of {U_{24}} (45 mg/mL) and {U_{60}} (85 mg/mL) in aqueous solution (top) and in the solid state (bottom).

(HOO^-) ion in aqueous solution, although the similar energies of this band and the Raman band of H_2O_2 (875 cm^{-1}) suggest that the 878 cm^{-1} band is the result of a uranyl−peroxide complex or a similar peroxo-containing species. The blue

dx.doi.org/10.1021/ic402570b | Inorg. Chem. 2014, 53, 1562−1569

shifting of the band suggests that there has been additional electron localization along the O−O internuclear axis relative to free H_2O_2 or HOO^-.

The band at 878 cm^{-1} vanishes upon addition of coordinating cations such as Na^+, but noncoordinating cations such as tetralkylammonium have no effect on the band intensity or position (Figure 5). The cation responsiveness of the band

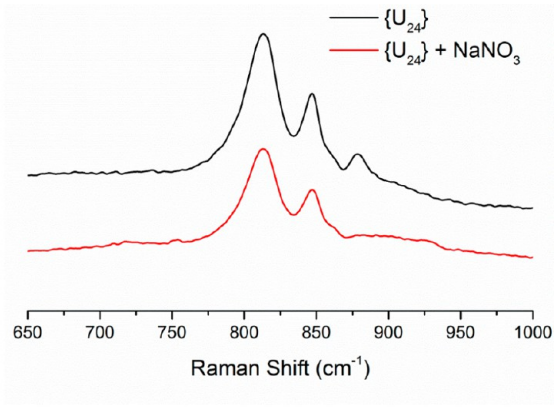

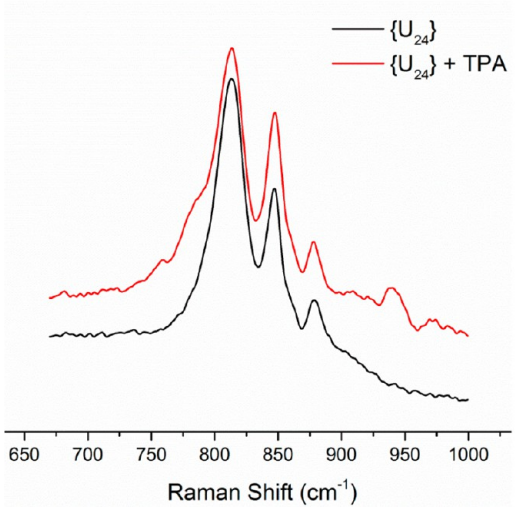

Figure 5. Top: Raman spectrum of $\{U_{24}\}$ in water and in 25 μM $NaNO_3$. Bottom: Raman spectra of $\{U_{24}\}$ in water and in 0.1 M TPACl.

suggests two possible origins: the cluster with near-stoichiometric quantities of coordinating counterions may exist with some (but not all) of its peroxo ligands in direct association with counterions, and the bands near 840 cm^{-1} would arise from this configuration. The 878 cm^{-1} band could then arise from the peroxo ligands that are not coordinated by counterions, and the presence of additional counterions would reduce or eliminate this state. Computational studies have shown that counterions can alter the electron distribution in uranyl peroxide clusters,[33] lending support to this scenario. The attenuation of this band in the solid state, which may be considered the upper limit of contact ion pairing, lends support to the assignment of the 878 cm^{-1} band to the symmetric stretching mode of a peroxo ligand that is not associated with a coordinating cation.

Electrospray Ionization-Mass Spectrometry. ESI-MS of $\{U_{24}\}$ from aqueous solution in the absence of any cosolvent or additional salts displays a base peak at 1876.24 m/z and smaller peaks with maxima at 1500.74, 1657.60, 2067.69, and 2545.39 m/z (Figure 6). The most striking feature of the spectrum is

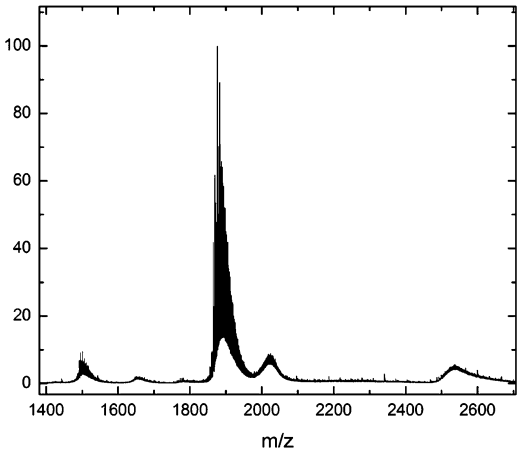

Figure 6. Negative-ion ESI mass spectrum of $\{U_{24}\}$ in water.

the peak widths, which dramatically exceed those of the simulated spectra (Figure 7), suggesting more complex gas-

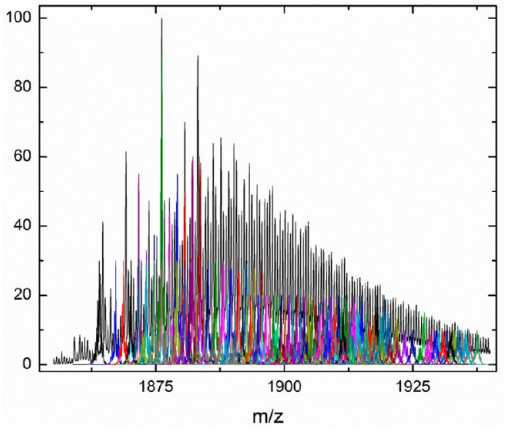

Figure 7. Detail of the base peak of the negative-ion mass spectrum of $\{U_{24}\}$ showing the convolution of isotope patterns. Simulated patterns are in color and appear beneath the measured spectrum.

phase speciation than would be expected from a simple ion-exchange and protonation process observed for mixed-counter-ion polyoxoniobates and polyoxotungstates.[9,15] These peaks are all asymmetric, with the most abundant species in the low m/z portion of the peak, indicating that the clusters do not undergo full desolvation in the ion source. The peaks form at least two series of multiply charged ions, with the 2545.39, 1876.24, and 1500.74 peaks representing the 3−, 4−, and 5− states of the most abundant species in the gas phase, and the series 2067.69 and 1657.60 corresponding to the less-abundant species. Assignments of all peak centerlines are given in Table S1 (Supporting Information). As indicated above, the peaks in the ESI mass spectrum of $\{U_{24}\}$ are much too wide to be attributable only to the isotope patterns of the elements, and also require transposition of solution constituents. For $\{U_{24}\}$, these constituents are $[UO_2(O_2)_x(OH)_y]_m^{n-}$ ($4 \leq 2x + y \leq 6$, $n = m[2 - 2x - y]$) species, Li^+, OH^-, and H^+ from the Li^+ salt of $\{U_{24}\}$ and the water, and NO_3^- and Cl^- from cocrystallized constituents of their mother solutions.[37] The base peak of the

dx.doi.org/10.1021/ic402570b | Inorg. Chem. 2014, 53, 1562−1569

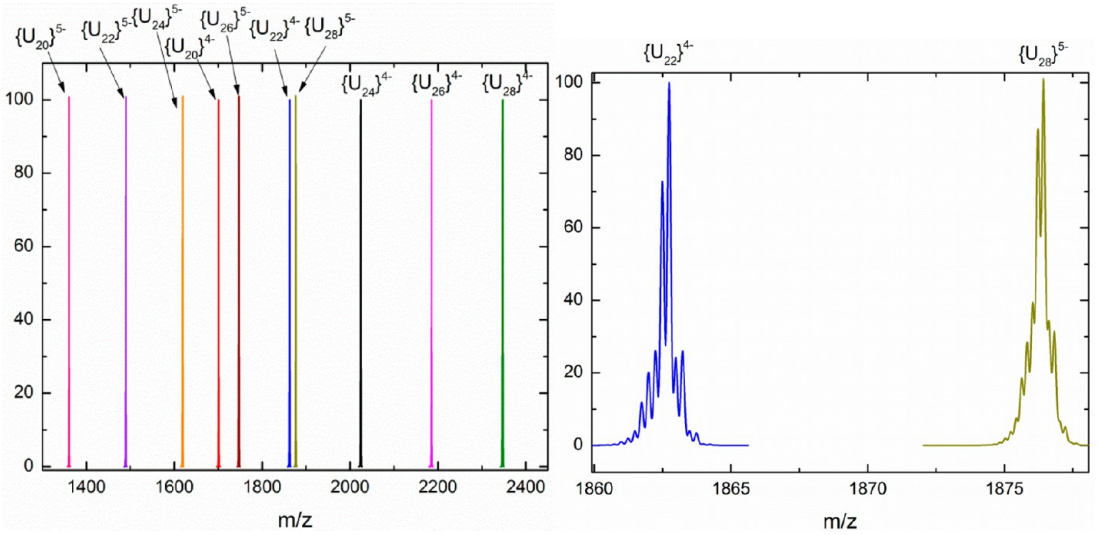

Figure 8. Left: Simulated mass spectra of ions of composition $\{[UO_2(O_2)(OH)]_nLi_xH_y(H_2O)_{12}\}^{m-}$ with mass-to-charge ratios near those observed for $\{U_{24}\}$- and $\{U_{24}\}$-derived species showing the ability to differentiate clusters with similar nuclearities; *n*, *x*, *y*, and *m* are defined as above. Right: Detail of the region containing $\{U_{22}\}^{4-}$ and $\{U_{28}\}^{5-}$ isotope patterns.

spectrum shows that the peak is not a single isotope distribution, but many convoluted isotope distributions.

The peak-to-peak spacing within the base peak of the $\{U_{24}\}$ spectrum corresponds to a 4− ion, and the minimum mass-to-charge ratio of a tetranegative $\{U_{24}\}$ species, that of $H_{20}\{U_{24}\}^{4-}$, assuming no in-source redox processes, is 1919.18. Therefore, the whole cluster can exist only in the high *m*/*z* region of the peak. The base peak must represent a fragment ion, rather than the whole $\{U_{24}\}$ cluster, although some contribution from this ion in the higher *m*/*z* region cannot be ruled out. The simulated isotope patterns used to model the composition of the peak represent a large series based on the $[UO_2(O_2)(OH)]_{22}^{22-}$ ion. The required charge is obtained by the addition of H^+ and Li^+, and the majority of peak broadening results from the hydration of the gas-phase species and transposition of neutral species and charge-balancing cations. The overall composition assigned to the base peak, $\{[UO_2(O_2)(OH)]_{22}H_xLi_{18-x}(H_2O)_{12-27}(Li_yH_{1-y}Cl)_{0-2}(Li_zH_{1-z}NO_3)_{0-2}(Li_qH_{1-q}OH)_{0-3}\}^{4-}$, accounts for the observed peak positions to within 0.03 *m*/*z* units. The observed intensities, however, are not weighted according to the abundance of species in solution, but rather by the kinetic stability of the ions (or ion/neutral species adducts) produced during the electrospray process over the time between the production of gas-phase species in the ion source and when the ions reach the detector. Fractional weights have been applied to the simulated spectra in Figure 7 to better represent the relative abundances of the proposed species. The weighting factors have been chosen to best account for the observed isotope patterns and intensities, but are not taken to represent the abundances of the constituent hydration and ion pairing states, or the identity of neutral species adducts in solution or the relative abundances of proposed species in the gas phase.

Despite the limitations due to ESI-MS peak broadening, unambiguous assignment of the nuclearity of the clusters is feasible even if it is difficult to differentiate between adjacent charge states (vide infra). Figure 8 shows the simulated mass spectra of clusters of composition $\{[UO_2(O_2)(OH)]_nLi_xH_y(H_2O)_{12}\}^{m-}$, where $x + y - n = m$ for $m = 4$, 5 and $n = 20-28$, even numbers only. To ensure the closest approximation of the centerlines of peaks derived from these ions, compositions with equal or nearly equal numbers of H^+ and Li^+ ions were used. The simulations are restricted to clusters of even numbers of uranium atoms because clusters with odd numbers of uranium atoms represent a very small fraction of known uranyl peroxide clusters.[20]

Of the species simulated, only two, $\{[UO_2(O_2)(OH)]_{22}Li_9H_9(H_2O)_{12}\}^{4-}$ and $\{[UO_2(O_2)(OH)]_{28}Li_{10}H_{13}(H_2O)_{12}\}^{5-}$, show maximum-to-maximum distances of less than 20 *m*/*z*. While both of these species will exist as parts of larger hydration and cation transposition series, the distribution for $\{U_{28}\}$ will be broader because it requires more cations to reach a comparable charge, and thus the pattern will show more peaks resulting from cation transposition. The two clusters can be further differentiated by other peaks in the spectrum, as the other charge states of these two clusters are well-separated.

The final problem for the interpretation of the mass spectra of uranyl peroxide clusters is the effective instrumental resolution (*R*), defined as the ratio of observed peak spacing (Δm) to the mass (m) at which the peaks are observed, expressed as

$$R = \frac{m}{\Delta m}$$

The charges adopted by uranyl peroxide clusters in the gas phase result in small distances between the peaks derived from different isotopomers. Ordinarily, this spacing is equal to the reciprocal of the charge on the ion. At large values of *m*/*z*, however, the factors that increase resolving power for small ions in time-of-flight (TOF) detectors can exaggerate other sources of error, such as the width of ion packets entering the quadrupole and the initial distribution of gas-phase ion velocities.[38] These limitations on resolution are particularly important for clusters larger than $\{U_{24}\}$, as the accurate determination of charge on the $\{U_{24}\}$ (and $\{U_{24}\}$-derived) species discussed above requires resolving powers of at least 7500, and the charge states of larger clusters such as $\{U_{60}\}$ cannot be unambiguously resolved at 10 000 resolving power. The interpretation of the mass spectra of clusters without the

dx.doi.org/10.1021/ic402570b | Inorg. Chem. 2014, 53, 1562−1569

aid of unambiguous charge state assignments is discussed below.

The ESI mass spectrum of $\{U_{60}\}$ (Figure 9) is much simpler than that of $\{U_{24}\}$. Instead of fragment ions as in the case of

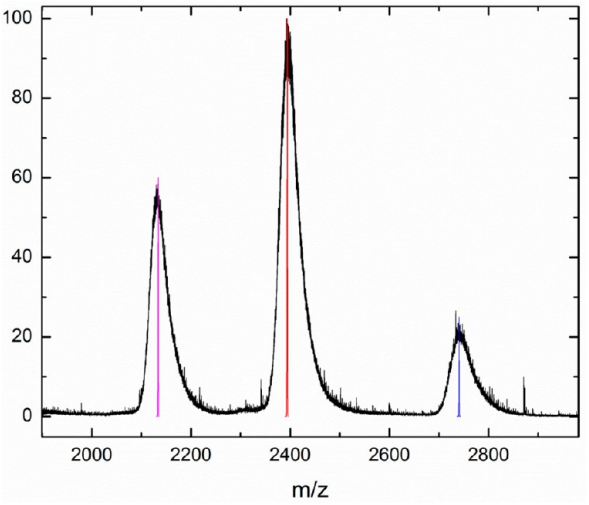

Figure 9. ESI mass spectrum of $\{U_{60}\}$ in water. The colored lines represent simulated species.

$\{U_{24}\}$, the centerlines are all assignable to multiple charge states of unfragmented $\{U_{60}\}$. One explanation for the observation that $\{U_{60}\}$ does not fragment in the way that $\{U_{24}\}$ does is because of the partitioning of Li^+ to the exterior of the cluster in solution.[39] Computational results have indicated that uranyl peroxide cage clusters are stabilized by cation coordination in the cluster's rings,[32,34] and the electrospray process may result in fragmentation of clusters that are not adequately stabilized by their counterions. The presence of K^+ in $\{U_{60}\}$ and both K^+ and Rb^+ in $\{U_{28}\}$ would then account for the transmission of the unfragmented clusters as the dominant species. This interpretation is supported by Li^+ sequestration using *N,N,N′N′*-tetramethylethylenediamine (TMEDA) (1% v/v in H_2O) as a selective Li^+ complexant. The mass spectrum of $\{U_{24}\}$ as the $(TMEDA)_2Li^+$ salt (Figure S5, Supporting Information) shows a base peak at 1282.96 *m/z* corresponding to the monoanion $[UO_2(O_2)(OH)]_4H_7^-$. Also visible are the penta- and hexa- or heptaanions of $\{U_{22}\}$ at 1534.47 and 1337.9 *m/z*, respectively. No peaks consistent with unfragmented $\{U_{24}\}$ are observed, strongly suggesting that intimate (i.e., inner-sphere) association with counterions is critical for cluster stability in the gas phase.

Similar to the mass spectrum of $\{U_{24}\}$, the line broadening in the spectrum of $\{U_{60}\}$ is attributed to loss and addition of neutral molecules (e.g., water, $LiNO_3$) as is the case for the spectrum of $\{U_{24}\}$, and the peak asymmetry resulting from the gradual decline in abundance species with higher degrees of neutral-species association. The proposed charge states are consistent with the peak positions, the peak-to-peak distance decreases with increasing charge, and the decrease is by the amount expected for changes between these charge states for a species the size of $\{U_{60}\}$. Assignments of peak centerlines are given in Table S2 (Supporting Information).

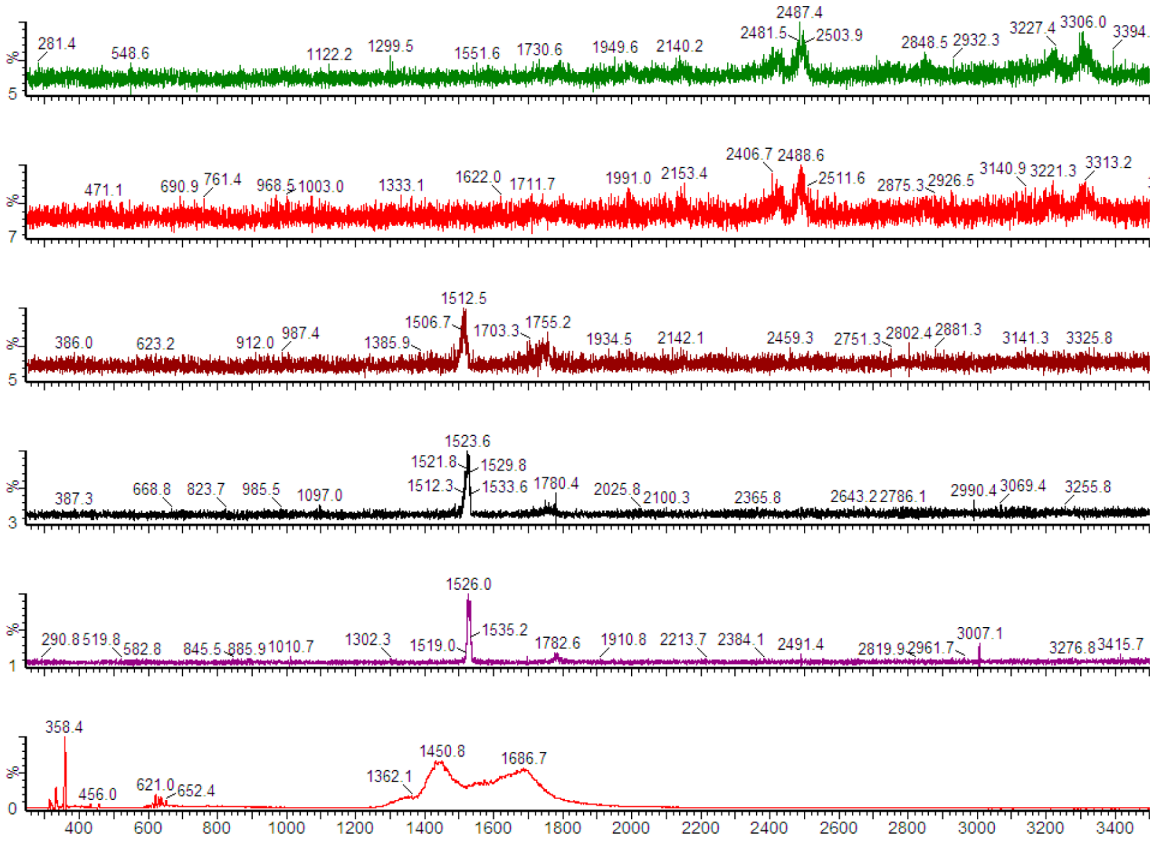

Figure 10. From bottom to top: ESI mass spectra of $\{U_{28}\}$ in water and MS/MS spectra derived from the parent at 1530 *m/z* with collision energies of 1, 10, 20, 35, and 40 eV.

dx.doi.org/10.1021/ic402570b | *Inorg. Chem.* 2014, 53, 1562−1569

The case of the mixed Rb^+/K^+ salt of $\{U_{28}\}^{21}$ provides another situation where determination of charge state is ambiguous. The low-resolution (triple quadrupole) mass spectrum of the cluster (Figure 10, bottom) displays overlapping peaks, ostensibly showing the hexa- and heptaanions of intact $\{U_{28}\}$ (centerline assignments are given in Table S3, Supporting Information). In this case, the presence of a single cluster and its identity are verified by tandem MS (MS/MS) experiments (Figure 10).

Isolation and fragmentation of the peaks at 1450.8 (Figure S1), 1530, and 1686.7 m/z (Figure S2) (Supporting Information) show two marked similarities: first, a minimum fragmentation energy of ca. 35 eV, and identical fragment ion peaks at 2411.7, 2487.4, 3227.4, and 3306.0 m/z. These mass-to-charge ratios correspond to the tri- and tetraanions of $\{U_{28}\}$, strongly suggesting not only the presence of the cluster but also that the whole cluster persists both in solution and in the gas phase. In addition, the formation of the same product ions from multiple parent ions with similar threshold energies strongly suggests that this behavior is characteristic of $\{U_{28}\}$, and can be used as the basis for identification of the cluster.

The MS/MS method can also be used to confirm the assignment of the base peak of the $\{U_{24}\}$ spectrum as belonging to the $\{U_{22}\}$ fragment discussed above. Isolation and fragmentation of the base peak with m/z = 1525.01 in the low-resolution spectrum (Figure S4, Supporting Information) gives a product-ion spectrum consisting of two peaks at 1423 and 1774 m/z. These peaks correspond to the base peak species in its initial (5−) charge state, but with fewer neutral adducts (1423 m/z, $[\{U_{22}\}(H_2O)_3Li_4H_{13}]^{5-}$) and the same cluster in a lower charge state (1774 m/z, $[\{U_{22}\}(H_2O)\text{-}Li_7H_{11}]^{4-}$).

CONCLUSION

We have demonstrated Raman and ESI-MS methods for the noncrystallographic characterization of uranyl peroxide clusters. These methods are amenable to study reaction mixtures without crystallization, hopefully leading to an enhanced ability to study these molecules and their reactivity. The Raman studies suggest significant covalent bonding within the clusters consistent with earlier simulations, and the relative positions of the Raman bands for the symmetric stretching modes of the uranyl ion and peroxo ligands appear to be general.

ASSOCIATED CONTENT

Supporting Information

Additional ESI-MS and MS/MS spectra. This material is available free of charge via the Internet at http://pubs.acs.org.

AUTHOR INFORMATION

Corresponding Author

*E-mail: pburns@nd.edu.

Notes

The authors declare no competing financial interest.

ACKNOWLEDGMENTS

This research is funded by the Office of Basic Energy Sciences of the U.S. Department of Energy as part of the Materials Science of Actinides Energy Frontiers Research Center (DE-SC0001089). Chemical analyses were conducted at the Center for Environmental Science and Technology at the University of Notre Dame. Electrospray ionization mass spectra were collected at the Mass Spectrometry and Proteomics Facility at the University of Notre Dame. Raman spectra were collected at the Materials Characterization Facility of the Center for Sustainable Energy at the University of Notre Dame.

REFERENCES

(1) Anslyn, E. V.; Dougherty, D. A. *Modern Physical Organic Chemistry*; University Science Books: South Orange, NJ, 2005.
(2) Taft, R. W.; Deno, N. C.; Skell, P. S. *Annu. Rev. Phys. Chem.* **1957**, *9*, 287−314.
(3) Ginsberg, A. P., Ed. *Inorganic Syntheses*; John Wiley & Sons, Inc.: Hoboken, NJ, 1990; Vol. *27*.
(4) Anderson, T. M.; Hill, C. L. *Inorg. Chem.* **2002**, *41*, 4252−4258.
(5) Weinstock, I. A.; Cowan, J. J.; Barbuzzi, E. M. G.; Zeng, H.; Hill, C. L. *Inorg. Chem.* **1999**, 4608−4617.
(6) Neiwert, W. A.; Cowan, J. J.; Hardcastle, K. I.; Hill, C. L.; Weinstock, I. A. *Inorg. Chem.* **2002**, *41*, 6950−6952.
(7) Sundaram, K. M.; Neiwert, W. A.; Hill, C. L.; Weinstock, I. A. *Inorg. Chem.* **2006**, *45*, 958−960.
(8) Villa, E. M.; Ohlin, C. A.; Casey, W. H. *J. Am. Chem. Soc.* **2010**, *132*, 5264−5272.
(9) Villa, E. M.; Ohlin, C. A.; Balogh, E.; Anderson, T. M.; Nyman, M. D.; Casey, W. H. *Angew. Chem., Int. Ed.* **2008**, *47*, 4844−4846.
(10) Ohlin, C. A. *Chem.—Asian J.* **2012**, *7*, 262−270.
(11) Miras, H. N.; Wilson, E. F.; Cronin, L. *Chem. Commun.* **2009**, 1297−311.
(12) Thiel, J.; Ritchie, C.; Streb, C.; Long, D.-L.; Cronin, L. *J. Am. Chem. Soc.* **2009**, *131*, 4180−4181.
(13) Ohlin, C. A.; Villa, E. M.; Fettinger, J. C.; Casey, W. H. *Angew. Chem., Int. Ed.* **2008**, *47*, 8251−8254.
(14) Wilson, E. F.; Abbas, H.; Duncombe, B. J.; Streb, C.; Long, D.-L.; Cronin, L. *J. Am. Chem. Soc.* **2008**, *130*, 13876−13884.
(15) Cao, J.; Li, C.; Zhang, Z.; Xu, C.; Yan, J.; Cui, F.; Hu, C. *J. Am. Soc. Mass Spectrom.* **2012**, *23*, 366−374.
(16) Johnson, G. E.; Al Hasan, N. M.; Laskin, J. *Int. J. Mass Spectrom.* **2013**, *354*−*355*, 333−341.
(17) Vila-Nadal, L.; Rodriguez-Fortea, A.; Yan, L.-K.; Wilson, E. F.; Cronin, L.; Poblet, J. M. *Angew. Chem., Int. Ed.* **2009**, *48*, 5452−5456.
(18) Vila-Nadal, L.; Wilson, E. F.; Miras, H. N.; Rodriguez-Fortea, A.; Cronin, L.; Poblet, J. M. *Inorg. Chem.* **2011**, *50*, 7811−7819.
(19) Armstrong, C. R.; Nyman, M.; Shvareva, T.; Sigmon, G. E.; Burns, P. C.; Navrotsky, A. *Proc. Natl. Acad. Sci. U.S.A.* **2012**, *109*, 1874−1877.
(20) Qiu, J.; Burns, P. C. *Chem. Rev.* **2013**, *113*, 1097−1120.
(21) Nyman, M.; Rodriguez, M. A.; Alam, T. M. *Eur. J. Inorg. Chem.* **2011**, 2197−2205.
(22) Unruh, D. K.; Burtner, A.; Pressprich, L.; Sigmon, G. E.; Burns, P. C. *Dalton Trans.* **2010**, *39*, 5807−5813.
(23) Sigmon, G. E.; Ling, J.; Unruh, D. K.; Moore-Shay, L.; Ward, M.; Weaver, B.; Burns, P. C. *J. Am. Chem. Soc.* **2009**, *131*, 16648−16649.
(24) Sigmon, G. E.; Weaver, B.; Kubatko, K.-A.; Burns, P. C. *Inorg. Chem.* **2009**, *48*, 10907−10909.
(25) Burns, P. C.; Kubatko, K.-A.; Sigmon, G.; Fryer, B. J.; Gagnon, J. E.; Antonio, M. R.; Soderholm, L. *Angew. Chem., Int. Ed.* **2005**, *44*, 2135−9.
(26) Sigmon, G. E.; Burns, P. C. *J. Am. Chem. Soc.* **2011**, *133*, 9137−9139.
(27) Kubatko, K.-A.; Burns, P. C. *Inorg. Chem.* **2006**, *45*, 6096−6098.
(28) Burns, P. C.; Hughes, K.-A. *Am. Mineral.* **2003**, *88*, 1165−1168.
(29) Monroe, M. *Molecular Weight Calculator*, Pacific Northwest National Laboratory: Richland, WA, v6.49; 2012.
(30) Bastians, S.; Crump, G.; Griffith, W. P.; Withnall, R. *J. Raman Spectrosc.* **2004**, *35*, 726−731.
(31) Zazhogin, A. A.; Lutz, H. D.; Komyak, A. I. *J. Mol. Struct.* **1999**, *482*−*483*, 189−193.
(32) Vlaisavljevich, B.; Gagliardi, L.; Burns, P. C. *J. Am. Chem. Soc.* **2010**, *132*, 14503−14508.

(33) Miro, P.; Bo, C. *Inorg. Chem.* **2012**, *20*, 3840−3845.
(34) Pierrefixe, S.; Bo, C. *J. Am. Chem. Soc.* **2010**, *38*, 17787−17794.
(35) McGlynn, S. P.; Smith, J. K.; Neely, W. C. *J. Chem. Phys.* **1961**, *35*, 105−116.
(36) Johnson, R. L.; Ohlin, C. A.; Pellegrini, K.; Burns, P. C.; Casey, W. H. *Angew. Chem., Int. Ed.* **2013**, *52*, 7464−7467.
(37) Verhoeff, A. A.; Kistler, M. L.; Bhatt, A.; Pigga, J.; Groenewold, J.; Klokkenburg, M.; Veen, S.; Roy, S.; Liu, T.; Kegel, W. K. *Phys. Rev. Lett.* **2007**, *066104*, 066104.
(38) Chernushevich, I. V; Loboda, A. V.; Thomson, B. A. *J. Mass Spectrom.* **2001**, *36*, 849−865.
(39) Nyman, M.; Alam, T. M. *J. Am. Chem. Soc.* **2012**, *134*, 20131−20138.
(40) Qiu, J.; Nguyn, K.; Jouffret, L. J.; Szymanowski, J. E. S.; Burns, P. C. *Inorg. Chem.* **2013**, *52*, 337−345.